






Cite this: DOI: 10.1039/c8nj05883k

# Selective electrochemical detection of bisphenol A using a molecularly imprinted polymer nanocomposite†

Haydar Ali,  Soumita Mukhopadhyay  and Nikhil R. Jana \*

Bisphenol A is the most common endocrine disrupting chemical found in the environment and human exposure to it leads to a variety of health issues. Thus detection and removal of bisphenol A from industrial waste/soil/drinking water are critical to minimize human consumption. Here we report a molecularly imprinted nanocomposite for selective electrochemical detection of bisphenol A. The nanocomposite has covalently connected polyacrylate,  $\beta$ -cyclodextrin and reduced graphene oxide components with the molecular imprints of bisphenol A for its selective capture *via* host–guest complexation with  $\beta$ -cyclodextrin. Bisphenol A can be selectively detected in the presence of various bisphenol A analogues *via* an electrochemical approach where the reduced graphene oxide component induces electrocatalysis. The linear concentration range of bisphenol A detection is 0.02–1.0  $\mu\text{M}$  with a limit of detection (LOD) of 8 nM. This approach has been used for the detection of bisphenol A in contaminated water and may be extended to the detection of bisphenol A among other natural contaminants.

Received 20th November 2018,  
Accepted 5th December 2018

DOI: 10.1039/c8nj05883k

rsc.li/njc

## Introduction

Bisphenol A is the most common endocrine disrupting chemical found in nature. Bisphenol A enters the environment from polycarbonate plastics and epoxy pitches utilized in industrial and consumer products.<sup>1–8</sup> In particular, it contaminates soil and water through various procedures of industrial manufacture, industrial wastes and leaching from disposed bisphenol A-based items (*e.g.* plastic jugs, toys, packages, and papers). Human consumption of bisphenol A leads to a variety of issues such as birth defects, infertility, obesity and prostate cancer.<sup>2–5,7,8</sup> Thus detection, separation and degradation of bisphenol A from industrial waste, soil, and drinking water are important for decreased human consumption.<sup>6,9–13</sup>

The molecular imprinting approach is a broadly utilized strategy to accomplish molecular recognition in a composite *via* target molecule assisted assembly.<sup>14–29</sup> In this approach polymerization or composite formation is performed in the presence of a target molecule as a template so that the polymeric network produces the recognition sites (or imprints) of the target molecule, even after the target/template is removed. Many molecularly imprinted materials have been designed for the

specific identification of target molecules. Examples of molecularly imprinted materials include a mesoporous silica–quantum dot–polymer hybrid,<sup>21</sup> an exfoliated graphene embedded hybrid matrix,<sup>22</sup> phenylboronic acid functionalized mesoporous silica,<sup>23</sup> polymer microspheres,<sup>24</sup> cyclodextrin based materials<sup>15,26,27</sup> and graphene based materials.<sup>28,29</sup> These molecularly imprinted composites have been utilized for the detection of tetracycline,<sup>21</sup> rhodamine 6G,<sup>22</sup> saccharides,<sup>23</sup> nicotine,<sup>24</sup> benzylparaben<sup>27</sup> and 17 $\beta$ -estradiol.<sup>29</sup>

The molecular imprinting approach coupled with different analytical techniques, namely, surface enhanced Raman spectroscopy (SERS),<sup>22,24</sup> fluorescence<sup>23,25</sup> and electrochemical approaches,<sup>19,30–39</sup> has been utilized for bisphenol A detection. In particular, the electrochemical method offers good sensitivity with short analysis time and requires inexpensive equipment. Hence, electrochemical detection of bisphenol A using a molecular imprinting platform has become an emerging research front where molecular imprinting offers selective capture of bisphenol A and the electrochemical method offers cost effective and sensitive detection of bisphenol A. For example, a molecularly imprinted TiO<sub>2</sub> single crystal is developed for bisphenol A detection in the 0.01–20  $\mu\text{M}$  concentration range,<sup>19</sup> molecularly imprinted polymer–graphitic carbon nitride is used for photo-electrocatalytic detection of bisphenol A in the 5–100  $\mu\text{M}$  concentration range,<sup>30</sup> a carbon nanotube–silica based molecularly imprinted material has been developed for electrochemical detection of bisphenol A in the micro- to nanomolar concentration range<sup>36</sup> and a gold nanoparticle–polymer-based molecularly

Centre for Advanced Materials and School of Materials Science, Indian Association for the Cultivation of Science, Kolkata-700032, India. E-mail: camrj@iacs.res.in

† Electronic supplementary information (ESI) available: Details of the characterization of nanocomposites and electrochemical detection and selectivity data of bisphenol A. See DOI: 10.1039/c8nj05883k

imprinted composite is reported for electrochemical detection of bisphenol A in the micro- to nanomolar concentration range.<sup>39</sup> These works show that the molecular imprinting approach appears very promising for selective detection of bisphenol A; however, reliability and sensitivity need to be improved further.

Here we report a molecularly imprinted nanocomposite composed of a covalently connected 3D network of reduced graphene oxide,  $\beta$ -cyclodextrin and polyacrylate that can be used for selective electrochemical detection of bisphenol A. It is synthesized under the host-guest complexation condition between  $\beta$ -cyclodextrin and bisphenol A and thus the molecular imprint of bisphenol A is present in the 3D network of the nanocomposite. The nanocomposite selectively captures bisphenol A in the presence of bisphenol A analogues and the adjacent reduced graphene oxide component offers electrocatalytic detection. The advantage of the presented method is that it utilizes a combined approach of molecular imprinting for selective capture of bisphenol A and a cost effective electrochemical method, as compared to other conventional analysis techniques, for sensitive detection of bisphenol A. Hence, this approach offers rapid analysis of bisphenol A in real water samples in the presence of other abundant common organic materials. Although reduced graphene oxide and  $\beta$ -cyclodextrin are extensively investigated, the combination of reduced graphene oxide and  $\beta$ -cyclodextrin in molecular imprinting-based bisphenol A detection and use of  $\beta$ -cyclodextrin acrylate in the synthesis of this molecularly imprinted nanocomposite has never been explored. The advantage of this combination is that it offers molecular imprinting by the  $\beta$ -cyclodextrin component for selective capture of bisphenol A followed by electrochemical detection by the reduced graphene oxide component.

## Experimental

### Materials

Graphite powder (< 20  $\mu\text{m}$ ), acrylamide (AAM),  $N,N'$ -methylene-bis-acrylamide (MBAA), ammonium persulfate (APS),  $N,N,N',N'$ -tetramethylethylenediamine (TMEDA), bisphenol A, hydrazine hydrate (64%), phenol, resorcinol, bromophenol blue (BPB), 4,4'-dihydroxybiphenyl (DHBP), and 4,4'-(hexafluoroisopropylidene)diphenol (BPAF) were purchased from Sigma Aldrich. Potassium permanganate ( $\text{KMnO}_4$ ), sodium nitrate ( $\text{NaNO}_3$ ) and hydrogen peroxide (30%) were purchased from Merck.

### Instrumentation

Transmission electron microscopy (TEM) samples were prepared by setting a drop of nanocomposite suspension on a carbon-covered copper grid and observed with a FEI Tecnai G2 F20 microscope. UV-visible absorption spectra of the samples were collected utilizing a Shimadzu UV-2550 spectrophotometer. Raman spectra with a 785 nm excitation laser were collected utilizing an Agiltron R3000 Raman spectrometer. XRD of the samples was performed on a Bruker D8 Advance powder diffractometer, by utilizing  $\text{Cu K}\alpha$  ( $\lambda = 1.54 \text{ \AA}$ ) as the incident radiation. Thermogravimetric analysis (TGA) of the samples was performed using a TA

instrument (SDT Q600). High resolution mass spectra (HRMS) were recorded using a Waters QTOF Micro YA263 spectrometer.

### Preparation of graphene oxide

Colloidal graphene oxide was synthesized by a modified Hummer's method as described earlier.<sup>6</sup> In brief, 100 mg graphite powder and 50 mg sodium nitrate were blended with 3 mL concentrated sulphuric acid in a beaker. The solution was cooled to 0  $^\circ\text{C}$  and 300 mg of  $\text{KMnO}_4$  was added stepwise. After thirty minutes, 10 mL water was added in two stages and the mixture was cooled to room temperature followed by addition of 100  $\mu\text{L}$  of 3%  $\text{H}_2\text{O}_2$  to consume excess permanganate. The solid was washed with hot water thoroughly, collected by low speed centrifugation (at 3000 rpm), air dried and dispersed in distilled water by sonication. Next, the solution was centrifuged at 3000 rpm to remove larger particles and the supernatant was utilized as a colloidal GO solution with a concentration of 1  $\text{mg mL}^{-1}$ .

### Synthesis of $\beta$ -cyclodextrin acrylate

First, 1.134 g  $\beta$ -cyclodextrin was dissolved in dry DMF and 1.6 mL of triethylamine was added under inert conditions. Next, 96  $\mu\text{L}$  of crotonyl chloride (equivalent of cyclodextrin) was added and the mixture was warmed at 80  $^\circ\text{C}$  overnight. After that, diethylether was added into the mixture and washed with acetone several times to expel the unreacted precursor. The precipitate was air dried and utilized for further application. The formation of  $\beta$ -cyclodextrin acrylate was confirmed using mass spectroscopy (ESI,† Fig. S1).

### Preparation of a molecularly imprinted polymeric nanocomposite (MIPN)

At first, a  $\beta$ -cyclodextrin acrylate-bisphenol A inclusion complex was prepared by mixing them in 2 mL water. Typically, 40 mg or 20 mg  $\beta$ -cyclodextrin acrylate and 3.8 mg bisphenol A were used at their molar ratios of 2:1 and 1:1. In addition, amounts of AAM and MBAA were also varied, as shown in Table S1 (ESI†). Next, this mixed solution was added into 2 mL colloidal graphene oxide solution (concentration  $\sim 1 \text{ mg mL}^{-1}$ ). Next, 20  $\mu\text{L}$  of 25%  $\text{NH}_3$  solution was added with consistent stirring for 2 h. Next, 20  $\mu\text{L}$  hydrazine monohydrate solution was added and warmed at 70  $^\circ\text{C}$  for 15 min. The brown solution turns black within 10–15 min with the appearance of black precipitates. The precipitates were washed with water to remove unbound  $\beta$ -cyclodextrin acrylate (but not bisphenol A, as it is not water soluble) and then dispersed in water *via* sonication. Next, 50 mg acrylamide and 10 mg MBAA were mixed with continuous stirring. Next, 100  $\mu\text{L}$  of TMEDA and 5 mg APS were added with consistent stirring for 1 h. Next, the nanocomposite was isolated by centrifugation and washed with acetone several times for complete removal of bisphenol A and unreacted monomers. The removal of bisphenol A was examined by UV-absorbance study along with HPLC as shown in Fig. S2 (ESI†). From the figure it was observed that the absorbance peak of bisphenol A at  $\sim 276 \text{ nm}$  was diminished, confirming the successful removal of bisphenol A from the MIPN. After air drying, the nanocomposite was dispersed in water through sonication and utilized for further use. The non-imprinted

nanocomposite (NIPN) was synthesized *via* the same approach, except that bisphenol A was not used during synthesis. Three different sets of nanocomposites were prepared by varying the amount of  $\beta$ -cyclodextrin acrylate and acrylamide and they are designated as MIPN, MIPN1, MIPN2, NIPN, NIPN1, and NIPN2 (Table S1, ESI<sup>†</sup>).

### Electrochemical measurements

A glassy carbon electrode (GCE) 3 mm in diameter (surface area of 0.07 cm<sup>2</sup>) was cleaned successively utilizing 1, 0.3, and 0.05  $\mu$ m alumina powder, until the point that a mirror finish was obtained. Next, the electrode was ultrasonically cleaned with acetone and deionized water and dried in air at room temperature. Finally, the electrode was immersed in 0.5 M H<sub>2</sub>SO<sub>4</sub> and voltammetrically scanned from -0.4 to 1.2 V (*vs.* Ag/AgCl) at a rate of 100 mV s<sup>-1</sup> to clean the surface. Next, the MIPN/NIPN dispersion was dropped onto the GCE surface, dried in air at room temperature for 1 h and utilized for electrochemical measurements. Electrochemical measurements were performed with a CHI633D electrochemical analyzer in a conventional three-electrode system which was made out of a platinum wire as an auxiliary electrode, an Ag/AgCl/saturated KCl as a reference electrode and a modified GCE as a working electrode. All electrochemical experiments were performed at room temperature. For the electrochemical detection of bisphenol A, the cyclic voltammetry and differential pulse voltammograms (DPVs) were recorded at a sweep rate of 50 mV s<sup>-1</sup> using Britton–Robinson (BR) buffer at pH 4.0.

In order to investigate the bisphenol A detection selectivity, the glassy carbon electrode was modified with the MIPN or NIPN, separately. Next, the modified electrode was dipped into bisphenol A (1–20  $\mu$ M) solution in the presence of 5  $\mu$ M

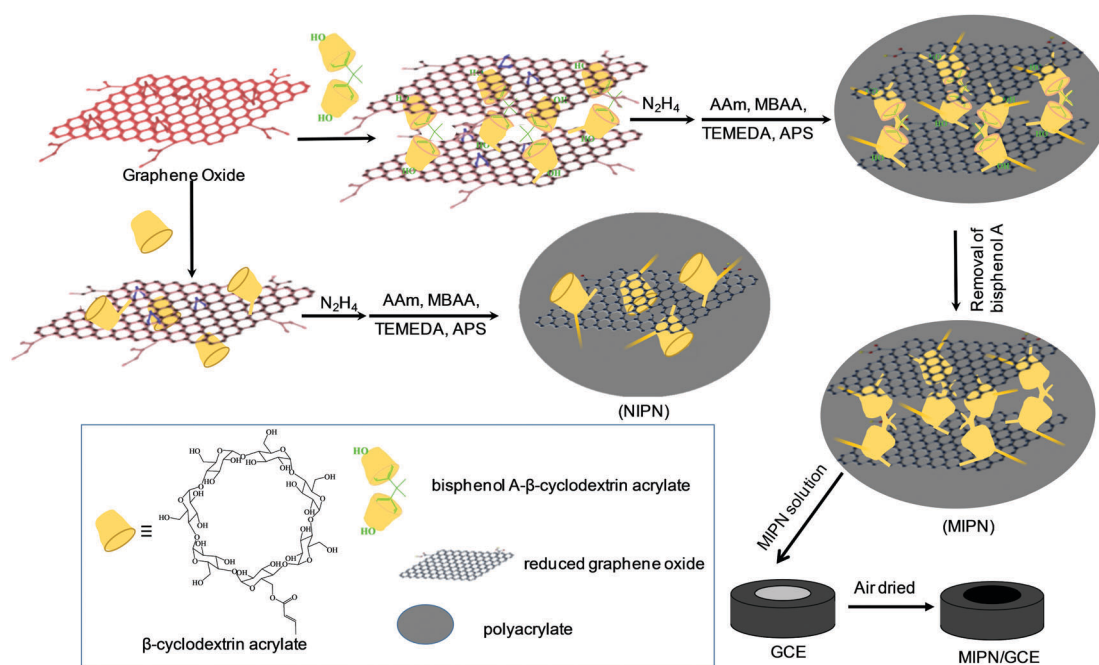
bisphenol A analogue solution (*viz.* phenol, resorcinol, BPB, BPAF and DHBP). The DPV was recorded at a sweep rate of 50 mV s<sup>-1</sup> in the range of 0.4 to 1.0 V and the peak current of bisphenol A was recorded. Efficient binding of the MIPN/NIPN with the glassy carbon electrode is expected due to the similar chemical properties of graphene and glassy carbon and is evident from the reproducible/intact electrochemical signal of bisphenol A, even after repeated measurements (see the Results section).

## Results and discussion

### Synthesis and characterization of molecularly imprinted polymeric nanocomposites (MIPNs)

The chemical structure of the molecularly imprinted nanocomposite and the approach for its synthesis are illustrated in Scheme 1. The nanocomposite has three components: reduced graphene oxide,  $\beta$ -cyclodextrin and polyacrylate. Reduced graphene oxide is selected due to its well known electrocatalytic properties and large surface area that can be used for functionalization.  $\beta$ -Cyclodextrin is selected as it is known to form an inclusion complex with bisphenol A by means of host–guest complexation.<sup>15</sup> The polyacrylate component offers porous and gel-like three dimensional networks with incorporated graphene and cyclodextrin. The three components are covalently linked to each other with porous and gel-like networks. The molecular recognition properties of the nanocomposite come from the selective incorporation of two phenolic components of bisphenol A with two adjacent cyclodextrins.

The synthesis approach has two steps. The first step involves reaction of graphene oxide with  $\beta$ -cyclodextrin acrylate in the



**Scheme 1** Schematic representation for the synthesis of a molecularly imprinted nanocomposite (MIPN) for bisphenol A and a non-imprinted nanocomposite (NIPN) and modification of electrodes for electrochemical measurements.

presence of bisphenol A. Under this condition bisphenol A forms an inclusion complex with  $\beta$ -cyclodextrin and the hydroxyl groups of  $\beta$ -cyclodextrin react with the epoxide groups of graphene oxide. The presence of epoxide groups on the graphene oxide surface is well known,<sup>40</sup> and extensive binding of cyclodextrin with graphene (which does not leach even after extensive washing) is indirect evidence of covalent binding between graphene oxide and cyclodextrin (see results below). Next, graphene oxide is converted to reduced graphene oxide (rGO) *via* reduction with hydrazine and then radical polymerization is performed in the presence of acrylamide and MBAA. Under this condition a porous nanocomposite is formed, incorporating the bisphenol A–cyclodextrin host–guest complex. Next, bisphenol A is extracted using organic solvent, leaving the molecularly imprinted nanocomposite (MIPN) in the solid form. The non-imprinted nanocomposite (NIPN) is

synthesized *via* the same approach, except that bisphenol A is not used during synthesis.

Details of structural characterization are summarized in Fig. 1 and Fig. S3–S5 (ESI<sup>†</sup>). The 3D structure along with a sheet morphology of rGO in the MIPN/NIPN is clearly seen in TEM images of the nanocomposites (Fig. 1a–d and Fig. S5, ESI<sup>†</sup>). Thermogravimetric analysis shows weight losses of about 16%, 47% and 51% in the temperature range between 100 and 800 °C for rGO, the MIPN and the NIPN, respectively (Fig. 1e). These weight losses are due to the functional groups and polymeric materials and the tentative amounts of polymeric materials present in the nanocomposites are ~31–35 wt% for the MIPN/NIPN. The amount of  $\beta$ -cyclodextrin in the nanocomposites has been estimated by an anthrone test and the amount comes to about 15–16 wt% for the MIPN/NIPN (Fig. 1f). XRD patterns show

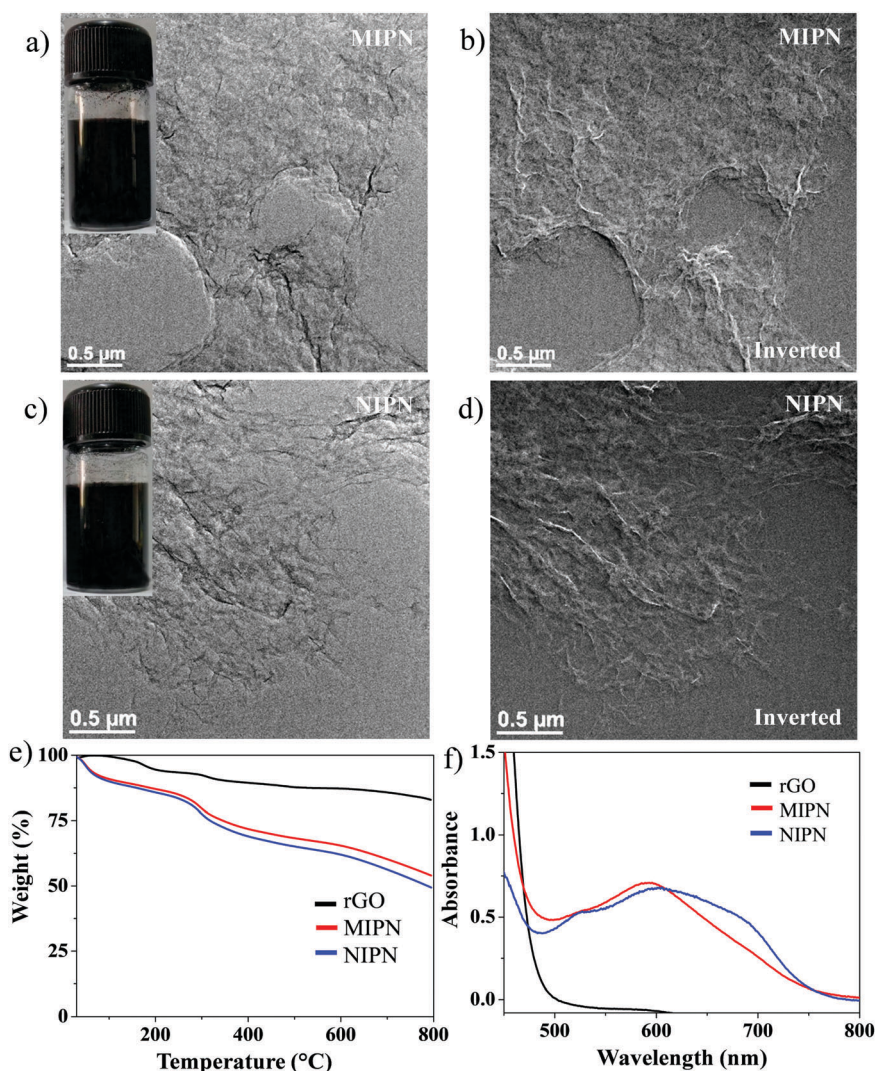


**Fig. 1** TEM image of the MIPN (a) along with the corresponding inverted image (b) and a TEM image of the NIPN (c) along with the corresponding inverted image (d), showing the 3D structure of the nanocomposites. Insets show colloidal dispersions of the MIPN/NIPN. (e) TGA curves of reduced graphene oxide (rGO), the MIPN and the NIPN, showing weight losses of 16 wt%, 47 wt% and 51 wt%, respectively, in the temperature range 100–800 °C. (f) Absorption spectra obtained after the anthrone test for rGO, the MIPN and the NIPN. These absorption spectra are used to estimate wt% of  $\beta$ -cyclodextrin bound to the composites (using the calibration graph obtained for varied  $\beta$ -cyclodextrin concentrations as  $Y = 2.5 \times 10^4 X + 0.1$  with  $R^2 = 0.99$ , where  $X$  is the molar concentration of  $\beta$ -cyclodextrin and  $Y$  is the absorbance at 610 nm).

characteristic reflections of rGO corresponding to (002) and (100) planes but the reflection corresponding to (100) becomes absent for the MIPN and NIPN due to the increased amorphous nature of the nanocomposite and the presence of polymeric layers (Fig. S3a, ESI†). SEM study does not provide much information on the 3D features of the rGO/nanocomposites (Fig. S3b, ESI†). The Raman spectra of the MIPN and NIPN show a prominent G band at  $\sim 1600\text{ cm}^{-1}$  and a D band at  $\sim 1300\text{ cm}^{-1}$  (Fig. S4a, ESI†). The intensity ratio of the D band to G band ( $I_D/I_G$ ) is 1.80 for the MIPN and 2.01 for the NIPN. These values are higher than that for rGO,<sup>41</sup> indicating the increased defects in the MIPN/NIPN due to the existence of the polymeric components. Compared to pure reduced graphene oxide, the MIPN shows some difference in TEM images, XRD and Raman spectra, which is attributed to the different chemical composition of the MIPN. However, the difference between the MIPN and NIPN is not detectable by TEM/XRD/Raman spectroscopy and is only observed during bisphenol A detection selectivity analysis (see results below).

The formation of host-guest complexation between  $\beta$ -cyclodextrin and bisphenol A is studied *via* UV-visible absorption spectroscopy (Fig. 2). The absorption band maximum of bisphenol A at 276 nm shifts by 5 nm after the inclusion complexation<sup>15</sup> and a similar result is also observed with the MIPN (Fig. 2a). This result suggests that  $\beta$ -cyclodextrin present in the MIPN also acts as host. We have also studied the stronger bisphenol A binding properties of the MIPN as compared to the NIPN. The same amount of the MIPN/NIPN is used to capture bisphenol A, and then washed samples are used to measure the absorption band of bisphenol A. The results show that the bisphenol A absorbance is strong for the MIPN, suggesting that the MIPN has stronger bisphenol A capturing properties, as compared to the NIPN (Fig. 2b).

### Selective electrochemical detection of bisphenol A

Electrochemical detection of bisphenol A is performed using a MIPN/NIPN modified glassy carbon electrode (GCE). For this purpose, cyclic voltammetry (CV) and differential pulse voltammetry (DPV) are carried out using various concentrations of bisphenol A. A typical voltammetric profile of bisphenol A at  $5\text{ }\mu\text{M}$  concentration is obtained for the MIPN/GCE and NIPN/GCE electrodes showing an irreversible anodic peak ( $E_{pa}$ ) at  $+0.74\text{ V}$  (Fig. S6a, ESI†). Very low peak current is observed for the NIPN/GCE (whereas no such peak is observed for the bare rGO/GCE), which suggests a poor electrochemical behaviour of bisphenol A for oxidation at lower concentration. In order to further assess the sensitivity of the MIPN and NIPN towards bisphenol A detection, besides CV study, DPV is also carried out using a wide range of concentrations of bisphenol A ( $20\text{--}0.02\text{ }\mu\text{M}$ ) as shown in Fig. 3 and Fig. S6b (ESI†). These results clearly depict a reproducible irreversible anodic peak at  $+0.74\text{ V}$ , due to the electro-active phenolic component of bisphenol A along with a trivial anodic peak that appears at  $\sim +0.5\text{ V}$ . This small peak ( $\sim +0.5\text{ V}$ ) corresponds to polymeric products; however, this signal is not reproducible and does not represent the bisphenol A concentration. Minute observation reveals that the MIPN modified electrode shows 20–25 times enhanced

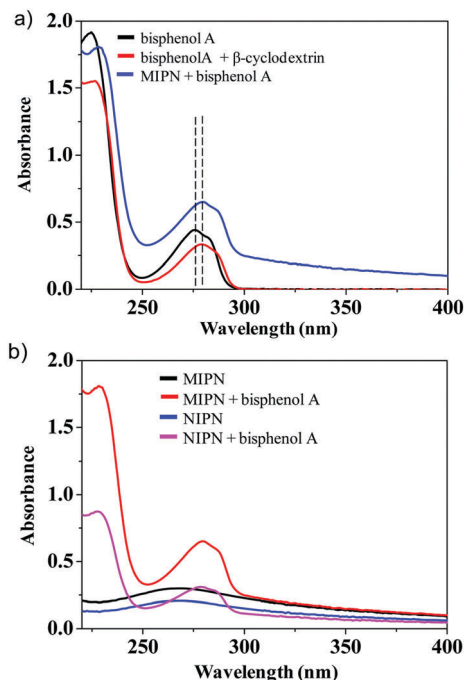


Fig. 2 (a) UV-visible absorption spectra of bisphenol A in water before and after forming the inclusion complex with  $\beta$ -cyclodextrin or the MIPN, showing slight red shifting of the absorption band. (b) Evidence of stronger bisphenol A binding properties by the MIPN as compared to the NIPN. The same amount of the MIPN/NIPN ( $0.2\text{ mg mL}^{-1}$ ) is used to capture bisphenol A and then washed samples are used to measure the absorption band of captured bisphenol A.

sensitivity at  $+0.74\text{ V}$  with the clear peak current even at  $0.02\text{ }\mu\text{M}$  bisphenol A concentration. In contrast, the NIPN modified electrode fails to show peak current at  $<0.5\text{ }\mu\text{M}$  bisphenol A concentration. The higher peak current and better sensitivity of the MIPN modified electrode can be attributed to the formation of imprinted cavities inside the MIPN, which offers better capturing of bisphenol A. The control synthesis of the MIPN/NIPN using  $\beta$ -cyclodextrin (without acrylate functionalization) produces a weaker electrochemical signal, suggesting the important role of  $\beta$ -cyclodextrin acrylate in the formation of molecular imprinting sites (Fig. S6c and d, ESI†). Other sets of MIPNs (1 and 2) are also tested but the peak currents of bisphenol A at  $+0.74\text{ V}$  are less intense (Fig. S7 and S8, ESI†) and sensitivity is also very low compared to the MIPN as shown in Table S1 (ESI†). The well-defined anodic peak observed at  $+0.74\text{ V}$  indicates that the electrode response to bisphenol A is a typical irreversible oxidation reaction since no corresponding reduction peak is observed. It is worthwhile to mention that this oxidation current increases with increasing concentration of bisphenol A and increases more sharply for the MIPN/GCE as compared to the NIPN/GCE. This can be attributed to the selective recognition of bisphenol A with the MIPN modified electrode, which on sweeping the electrode potential ultimately results in the bisphenol A oxidation at a particular potential. The linear concentration range of bisphenol A detection by the MIPN is determined to be  $0.02\text{--}1.0\text{ }\mu\text{M}$  with a LOD of  $8\text{ nM}$ .

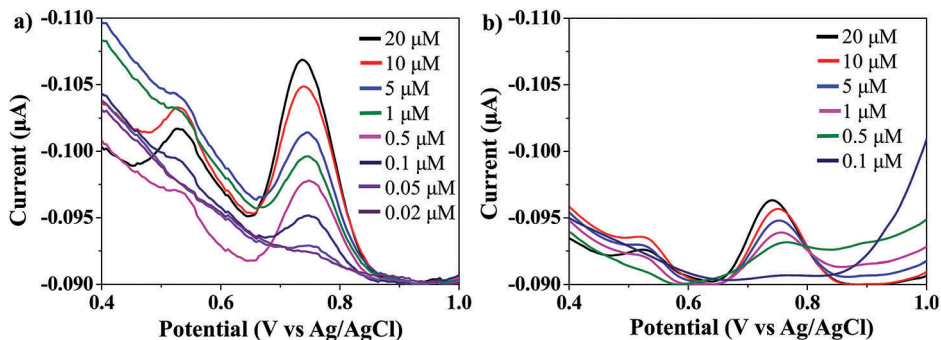


Fig. 3 Differential pulse voltammograms (DPVs) at various concentrations of bisphenol A using the GCE modified by the MIPN (a) and NIPN (b). The peak at  $\sim +0.74$  V corresponds to the bisphenol A oxidation peak.

(The linear fit equation is  $Y = -0.00119X - 0.0022$  with  $R^2 = 0.98$ , where  $Y$  is the current in  $\mu\text{A}$  and  $X$  is the concentration of bisphenol A in  $\mu\text{M}$ .) This sensitivity is comparable with the reported molecular imprinting-based bisphenol A detection methods (Table S2, ESI<sup>†</sup>).

In order to investigate the role of non-specific interaction in bisphenol A detection, an electrochemical study is performed

in a surfactant (Tween 80) solution. However, the results show little decrease in peak current at +0.74 V but the difference in sensitivity between the MIPN and NIPN remains unaltered (Fig. S9, ESI<sup>†</sup>). These results suggest that the enhanced detection sensitivity of the MIPN does not arise from the simple presence of functional components, rather their arrangement and orientation play a pivotal role.

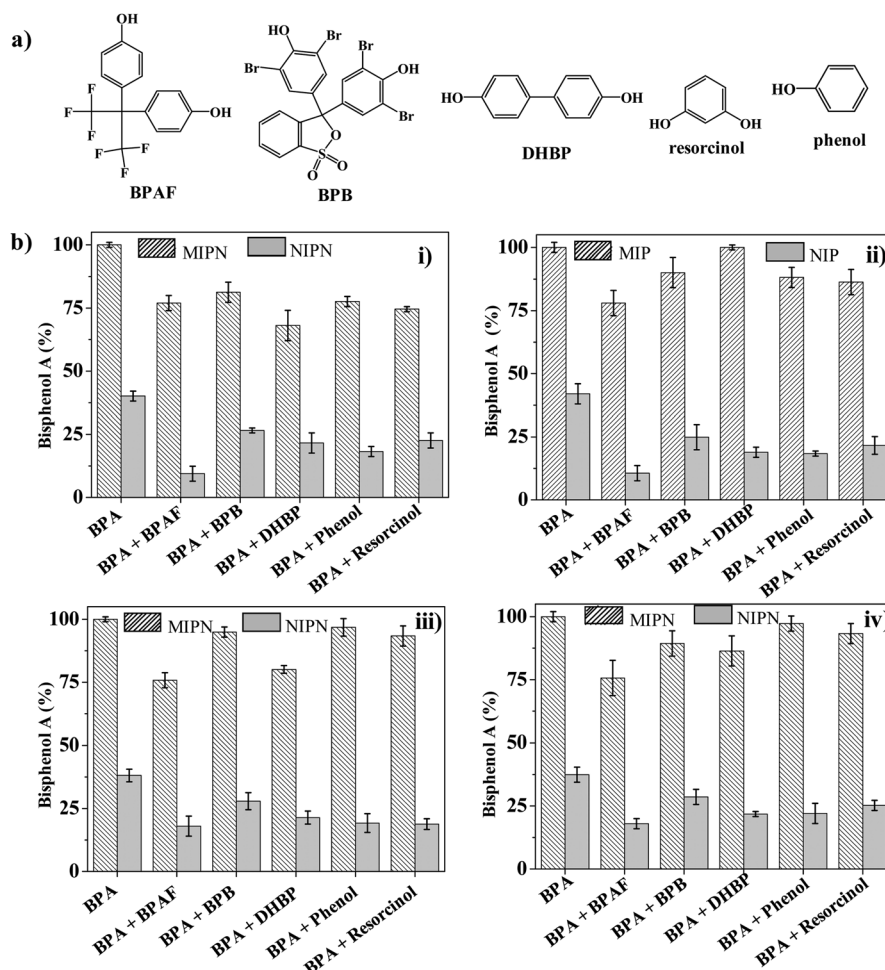


Fig. 4 (a) Molecular structures of bisphenol A analogue micropollutants that are used for selectivity tests. (b) Detection of bisphenol A (BPA) using the MIPN/NIPN modified electrodes in the presence of different bisphenol A analogues: (i) 1  $\mu\text{M}$  BPA, (ii) 5  $\mu\text{M}$  BPA, (iii) 10  $\mu\text{M}$  BPA and (iv) 20  $\mu\text{M}$  BPA. In all cases 5  $\mu\text{M}$  bisphenol A analogues are used and the detection is carried out by DPV. Error bars are the average of 3 measurements.

**Table 1** Electrochemical detection of bisphenol A in environmental samples with the MIPN/GCE<sup>a</sup>

Spiked level of BPA ( $\mu\text{M}$ )	Lake water		Tap water		Drinking water	
	Found ( $\mu\text{M}$ )	Recovery (%)	Found ( $\mu\text{M}$ )	Recovery (%)	Found ( $\mu\text{M}$ )	Recovery (%)
2	1.58 $\pm$ 0.2	78.9	1.75 $\pm$ 0.2	87.5	1.83 $\pm$ 0.1	91.5
5	3.56 $\pm$ 0.4	71.2	4.56 $\pm$ 0.4	91.2	4.78 $\pm$ 0.2	95.6
10	8.85 $\pm$ 0.5	88.2	8.27 $\pm$ 0.3	82.7	9.73 $\pm$ 0.2	97.3

<sup>a</sup> Average of five experimental data is shown for each measurement.

In order to accomplish bisphenol A detection selectivity by the MIPN over the NIPN, DPVs are also recorded in the presence of a wide concentration range of various bisphenol A analogues such as BPAF, BPB, DHBP, phenol and resorcinol (Fig. S10–S14, ESI<sup>†</sup>). These analogous micropollutants are selected based on their molecular size, arrangement of phenolic/aromatic moieties and hydrophobicity. The results show that the detection sensitivities to all the bisphenol A analogues are poor for both the MIPN and NIPN modified electrodes. In addition, it is observed that in some cases the MIPN shows poor sensitivity for the bisphenol A analogues, as compared to that of the NIPN. This result clearly suggests that the MIPN declines to selectively capture any of these bisphenol A analogues.

In the next experiment, the MIPN and NIPN modified electrodes are used for selective recognition of bisphenol A in the presence of bisphenol A analogues. As bisphenol A analogue micropollutants also produce signals near +0.74 V, we have used their lower concentrations so that the bisphenol A detection signal does not have any interference. In particular, we have used various bisphenol A concentrations (1–20  $\mu\text{M}$ ) in the presence of 5  $\mu\text{M}$  bisphenol A analogues (Fig. 4 and Fig. S15–S19, ESI<sup>†</sup>). The results clearly show that the bisphenol A peak current at +0.74 V decreases insignificantly in the case of the MIPN modified electrode, whereas the peak current at +0.74 V decreases significantly for the NIPN modified electrode. This result clearly suggests that bisphenol A can be selectively detected by the MIPN in the presence of the bisphenol A analogue micropollutants. Fig. 4 summarizes the MIPN/NIPN-based detection selectivities towards bisphenol A (1  $\mu\text{M}$ , 5  $\mu\text{M}$ , 10  $\mu\text{M}$ , and 20  $\mu\text{M}$ ) in the presence of 5  $\mu\text{M}$  solution of bisphenol A analogues. This study evidences the substantial fluctuation in bisphenol A signals for the NIPN as compared to higher bisphenol A signals along with low signal fluctuations for the MIPN. The higher sensing ability of the MIPN than that of the NIPN suggests that there are indeed imprinted cavities inside the material that are able to detect bisphenol A. However, for BPAF (the analyte with most chemical resemblance to bisphenol A), the significant binding affinity with the MIPN cannot be neglected. In contrast, the tolerance of the smaller bisphenol A analogues (*viz.* phenol, resorcinol and DHBP) further confirms that good binding can only be achieved when the analyte is comparable to the imprinted target molecule. It is noteworthy to mention that binding in the imprinted site of the MIPN/GCE occurs rapidly since the DPV study requires only <2 min.

Finally, we have used the MIPN to detect bisphenol A in water in the ample presence of other analogous micropollutants and also extended this work to the detection of bisphenol A in

various real water samples, namely, lake water, tap water and drinking water, for quantitative detection of bisphenol A following a standard spiking method (Table 1). It is observed that the recoveries (%) are quite high, which again confirms the efficacy of the MIPN and approves its candidature to be used as an efficient electrochemical sensor for the selective detection of bisphenol A.

## Conclusion

We report a designed molecularly imprinted nanocomposite for selective recognition and electrochemical detection of bisphenol A at micromolar concentration. The molecularly imprinted nanocomposite has three components, namely polyacrylate,  $\beta$ -cyclodextrin and reduced graphene oxide, which are covalently connected. It is synthesized under the host–guest complexation condition between  $\beta$ -cyclodextrin and bisphenol A so that the molecular imprint of bisphenol A is present in the 3D network of the nanocomposite. Thus bisphenol A is selectively captured in the presence of bisphenol A analogues and the adjacent reduced graphene oxide component offers electrocatalytic detection. This approach can be extended to the optical detection of bisphenol A or its selective separation.

## Conflicts of interest

The authors declare no competing financial interests.

## Acknowledgements

The authors acknowledge DST, Government of India, for financial assistance (No. DST/TM/WTI/2K16/02(G)) H. A. acknowledges CSIR, India, and S. M. acknowledges SERB-NPDF, India (No. PDF/2017/000173), for providing a research fellowship.

## References

- 1 J. Im and F. E. Löffler, *Environ. Sci. Technol.*, 2016, **50**, 8403–8416.
- 2 H.-J. Lehmler, B. Liu, M. Gadogbe and W. Bao, *ACS Omega*, 2018, **3**, 6523–6532.
- 3 J. K. Thomas, O. Birceanu, B. Sadoul and M. M. Vijayan, *Environ. Sci. Technol.*, 2018, **52**, 7951–7961.
- 4 M. Sonavane, P. Sykora, J. F. Andrews, R. W. Sobol and N. R. Gassman, *Chem. Res. Toxicol.*, 2018, **31**, 510–519.
- 5 L. Lu, T. Zhan, M. Ma, C. Xu, J. Wang, C. Zhang, W. Liu and S. Zhuang, *Environ. Sci. Technol.*, 2018, **52**, 6617–6625.

- 6 H. Ali and N. R. Jana, *Photochem. Photobiol. Sci.*, 2018, **17**, 628–637.
- 7 J. Moreman, O. Lee, M. Trznadel, A. David, T. Kudoh and C. R. Tyler, *Environ. Sci. Technol.*, 2017, **51**, 12796–12805.
- 8 T. T. Schug, A. F. Johnson, L. S. Birnbaum, T. Colborn, L. J. Guillette Jr., T. Crews, D. P. Collins, A. M. Soto, F. S. vomSaal, J. A. McLachlan, C. Sonnenschein and J. J. Heindel, *Mol. Endocrinol.*, 2016, **30**, 833–847.
- 9 M. Wang, Y. Shi, Y. Zhang, Y. Wang, H. Huang, J. Zhang and J. Song, *Electroanalysis*, 2017, **29**, 2620–2627.
- 10 R. Wang, K. Wu and C. Wu, *Anal. Methods*, 2015, **7**, 9261–9267.
- 11 Y. Guo, S. Guo, J. Ren, Y. Zhai, S. Dong and E. Wang, *ACS Nano*, 2010, **4**, 4001–4010.
- 12 A. Alsbaiee, B. J. Smith, L. Xiao, Y. Ling, D. E. Helbling and W. R. Dichtel, *Nature*, 2016, **529**, 190–194.
- 13 P. K. Kannon, C. Hu, H. Morgan, S. A. Moshkalev and C. S. Rout, *Nanotechnology*, 2016, **27**, 375504.
- 14 L. Chen, X. Wang, W. Lu, X. Wu and J. Li, *Chem. Soc. Rev.*, 2016, **45**, 2137–2211.
- 15 A. Kawamura, T. Kiguchi, T. Nishihata, T. Uragami and T. Miyata, *Chem. Commun.*, 2014, **50**, 11101–11103.
- 16 L. Chen, S. Xu and J. Li, *Chem. Soc. Rev.*, 2011, **40**, 2922–2942.
- 17 M. Yoshikawa, K. Tharpa and Ş.-O. Dima, *Chem. Rev.*, 2016, **116**, 11500–11528.
- 18 J. E. Lofgreen and G. A. Ozin, *Chem. Soc. Rev.*, 2014, **43**, 911–933.
- 19 D.-N. Pei, A.-Y. Zhang, X.-Q. Pan, Y. Si and H.-Q. Yu, *Anal. Chem.*, 2018, **90**, 3165–3173.
- 20 H. R. Culver, J. R. Clegg and N. A. Peppas, *Acc. Chem. Res.*, 2017, **50**, 170–178.
- 21 L. Zhang and L. Chen, *ACS Appl. Mater. Interfaces*, 2016, **8**, 16248–16256.
- 22 D. Carboni, Y. Jiang, M. Faustini, L. Malfatti and P. Innocenzi, *ACS Appl. Mater. Interfaces*, 2016, **8**, 34098–34107.
- 23 J. Tan, H.-F. Wang and X.-P. Yan, *Anal. Chem.*, 2009, **81**, 5273–5280.
- 24 T. Kamra, T. Zhou, L. Montelius, J. Schnadt and L. Ye, *Anal. Chem.*, 2015, **87**, 5056–5061.
- 25 Q. Li, T. Kamra and L. A. Ye, *Chem. Commun.*, 2016, **52**, 12237–12240.
- 26 H. A. Karoyo and D. L. Wilson, *Nanomaterials*, 2015, **5**, 981–1003.
- 27 S. Asman, S. Mohamad and N. Muhamad Sarih, *Int. J. Mol. Sci.*, 2015, **16**, 3656–3676.
- 28 J. Luo, J. Huang, J. Cong, W. Weiland and X. Liu, *ACS Appl. Mater. Interfaces*, 2017, **9**, 7735–7744.
- 29 F. Ning, H. Peng, J. Li, L. Chen and H. Xiong, *J. Agric. Food Chem.*, 2014, **62**, 7436–7443.
- 30 K. Yan, Y. Yang and J. A. Zhang, *Sens. Actuators, B*, 2018, **259**, 394–401.
- 31 Q. Yang, X. Wu, H. Peng, L. Fu, X. Song, J. Li, H. Xiong and L. Chen, *Talanta*, 2018, **176**, 595–603.
- 32 A. H. Kamel, X. Jiang, P. Li and R. A. Liang, *Anal. Methods*, 2018, **10**, 3890–3895.
- 33 F. Tan, L. Cong, X. Li, Q. Zhao, H. Zhao, X. Quan and J. Chen, *Sens. Actuators, B*, 2016, **233**, 599–606.
- 34 S. Dadkhah, E. Ziaei, A. Mehdinia, T. Baradaran Kayyal and A. Jabbari, *Microchim. Acta*, 2016, **183**, 1933–1941.
- 35 N. Ben Messaoud, A. Ait Lahcen, C. Dridi and A. Amine, *Sens. Actuators, B*, 2018, **276**, 304–312.
- 36 S. Güney and O. Güney, *Electroanalysis*, 2017, **29**, 2579–2590.
- 37 P. Deng, Z. Xu and Y. Kuang, *Food Chem.*, 2014, **157**, 490–497.
- 38 Y. Tan, J. Jin, S. Zhang, Z. Shi, J. Wang, J. Zhang, W. Pu and C. Yang, *Electroanalysis*, 2016, **28**, 189–196.
- 39 W.-R. Zhao, T.-F. Kang, L.-P. Lu, F.-X. Shen and S.-Y. Cheng, *J. Electroanal. Chem.*, 2017, **786**, 102–111.
- 40 D. R. Dreyer, S. Park, C. W. Bielawski and R. S. Ruoff, *Chem. Soc. Rev.*, 2010, **39**, 228–240.
- 41 A. Mondal and N. R. Jana, *Chem. Commun.*, 2012, **48**, 7316–7318.